tvst

Article

A Reflectivity Measure to Quantify Bruch's Membrane Calcification in Patients with Pseudoxanthoma Elasticum Using Optical Coherence Tomography

Sara Risseeuw[1], Edwin Bennink[2], Maarten G. Poirot[1], Pim A. de Jong[3], Wilko Spiering[4], Saskia M. Imhof[1], Redmer van Leeuwen[1], and Jeannette Ossewaarde-van Norel[1]

[1] Department of Ophthalmology, University Medical Center Utrecht, Utrecht University, Utrecht, The Netherlands
[2] Image Sciences Institute, University Medical Center Utrecht, Utrecht University, Utrecht, The Netherlands
[3] Department of Radiology, University Medical Center Utrecht, Utrecht University, Utrecht, The Netherlands
[4] Department of Vascular Medicine, University Medical Center Utrecht, Utrecht University, Utrecht, The Netherlands

Correspondence: Jeannette Ossewaarde-van Norel, Department of Ophthalmology, University Medical Center Utrecht, PO Box 85500, E 03.136, 3508 GA Utrecht, The Netherlands. e-mail: a.ossewaarde-vannorel@umcutrecht.nl

Received: January 6, 2020
Accepted: May 19, 2020
Published: July 23, 2020

Keywords: pseudoxanthoma elasticum; Bruch's membrane; calcification; reflectivity; quantification

Citation: Risseeuw S, Bennink E, Poirot MG, de Jong PA, Spiering W, Imhof SM, van Leeuwen R, Ossewaarde-van Norel J. A reflectivity measure to quantify bruch's membrane calcification in patients with pseudoxanthoma elasticum using optical coherence tomography. Trans Vis Sci Tech. 2020;9(8):34, https://doi.org/10.1167/tvst.9.8.34

Purpose: Progressive calcification of Bruch's membrane (BM) causes considerable visual morbidity in patients with pseudoxanthoma elasticum (PXE). Since calcification is hyperreflective on optical coherence tomography (OCT), our aim was to measure BM calcification with OCT imaging.

Methods: Case-control study with 45 patients with PXE under 40 years (range, 11–39) and 25 controls (range, 14–39). Spectralis HRA-OCT imaging consisted of seven macular B-scans with 250-µm spacing. Retinal segmentation was performed with the IOWA Reference Algorithms. MATLAB was used to extract and average z-axis reflectivity profiles. Layer reflectivities were normalized to the ganglion cell and inner plexiform layers. Both median and peak layer reflectivities were compared between patients with PXE and controls. The discriminative value of the retinal pigment epithelium (RPE)–BM peak reflectivity was analyzed using receiver operating characteristic analysis.

Results: The reflectivity profile of patients with PXE differed from controls in the outer retinal layers. The normalized median RPE-BM reflectivity was 41.1 (interquartile range [IQR], 26.3–51.9) in patients with PXE, compared with 22.5 (IQR, 19.3–29.5) in controls ($P = 2.09 \times 10^{-3}$). The normalized RPE-BM peak reflectivity was higher in patients with PXE (67.5; IQR, 42.1–84.2) than in controls (32.7; IQR, 25.7–38.9; $P = 2.43 \times 10^{-5}$) and had a high discriminative value with an area under the curve of 0.85 (95% confidence interval, 0.76–0.95). In patients with PXE under 40 years, increasing age did not have a statistically significant effect on the RPE-BM peak reflectivity (patients under 20 years: 44.2 [IQR, 40.5–74.6]; 20–30 years: 66.0 [IQR, 45.1–83.8]; 30-40 years: 70.8 [IQR, 49.0–88.0], $P = 0.47$).

Conclusions: BM calcification can be measured as increased RPE-BM reflectivity in young patients with PXE and has a high discriminative value.

Translational Relevance: In patients with PXE, the OCT reflectivity of Bruch's membrane may be the first biomarker for Bruch's membrane calcification and a valuable ophthalmologic endpoint in clinical trials.

Introduction

In patients with pseudoxanthoma elasticum (PXE), a rare disease with an estimated prevalence of at least 1:56,000, biallelic mutations of the *ABCC6* gene lead to ectopic mineralization in the vasculature, skin, and eyes.[1,2] Progressive calcification of Bruch's membrane (BM) initially presents as peau d'orange and typically causes formation of angioid streaks.[3] Eventually, this leads to significant visual morbidity at a relatively young age due to choroidal neovascularization (CNV)

Copyright 2020 The Authors

This work is licensed under a Creative Commons Attribution-NonCommercial-NoDerivatives 4.0 International License.

and macular atrophy.[4] Similar to geographic atrophy in age-related macular degeneration (AMD), macular atrophy in PXE can not be treated yet. A recent study has shown a beneficial effect of the bisphosphonate etidronate on vascular calcification.[5] In order to investigate the effect of etidronate and future potential treatments on retinal calcification, a reliable endpoint is warranted.

An increased reflectivity at the level of BM was observed on spectral domain optical coherence tomography (SD-OCT) in patients with PXE.[3,6,7] SD-OCT provides information on morphologic and reflective properties of tissues, which can be affected by increasing age or retinal disease.[8] The thickness of BM ranges from 2 to 5 µm,[9] which is comparable with the axial resolution of SD-OCT. Therefore, on SD-OCT, the BM cannot be distinguished from the above lying retinal pigment epithelium (RPE), and together these layers form the hyperreflective RPE-BM complex. It is plausible that the increased reflectivity of the RPE-BM complex on SD-OCT represents the calcification process in BM in patients with PXE. Therefore, the RPE-BM reflectivity may serve as a biomarker for the severity of PXE in the eye. However, commercial SD-OCT imaging is not developed to measure absolute reflectivity, and the measured reflectivity values are processed to create high-contrast images.[10] Also, patients with PXE frequently develop structural abnormalities such as CNV with increasing age, which may have different reflective properties than the cell layers of a healthy retina. Possibly, this causes attenuation of the OCT signal, and thereby it might alter the reflectivity values of underlying retinal layers, including the RPE-BM complex.[11]

We hypothesize that the reflectivity of BM may serve as a biomarker for retinal calcification in PXE. Our aim is to test this hypothesis by comparing the RPE-BM reflectivity on SD-OCT in young patients with PXE at an early disease stage with healthy controls.

Methods

Study Design and Population

This retrospective, observational case-control study was conducted at the University Medical Center Utrecht, The Netherlands, where the Dutch National Expertise Center for PXE is situated. The study adhered to the Declaration of Helsinki and its further amendments, and the study protocol was approved by the Institutional Ethics Committee (METC 19/257). We included patients with PXE aged under 40 years at the time of OCT measurement and who had a definitive diagnosis of PXE according to the Plomp criteria.[12] In total, 52 patients with PXE (104 eyes) were included. Our aim was to quantify the increased reflectivity due to calcification at the level of BM. Since the absolute reflectivity may be affected by acquisition parameters, quantification of reflectivity values requires normalization to other retinal layers.[8] The other retinal layers need to be intact and unaffected to ensure that the measured effect solely derives from BM calcification and is not due to differences in the optical properties of the other retinal layers. Therefore, for the purpose of this study, we first excluded all eyes with a best-corrected visual acuity below 0.9 decimals and subsequently all eyes with structural retinal pathology on SD-OCT to minimize a potential effect of a diseased retina on OCT reflectivity values.

Per eye, retinal imaging consisted of central and midperipheral color fundus photography (FF 450 plus; Carl Zeiss Meditec AG, Jena, Germany), 55° fundus autofluorescence, 55° near-infrared reflectance imaging (central and midperipheral), and macular SD-OCT (both Spectralis HRA-OCT; Heidelberg Engineering, Heidelberg, Germany). The images were systematically assessed by an experienced grader (SR) and graded as (1) only peau d'orange, (2) presence of angioid streaks, (3) CNV or fibrotic scarring, (4) macular atrophy, and (5) abnormalities on fundus autofluorescence or other abnormalities. Of these categories, eyes with only peau d'orange or presence of angioid streaks were included, since these abnormalities are inherent to BM calcification in patients with PXE and represent an early disease stage. The control group consisted of 25 age-matched controls (44 eyes) with no ophthalmic abnormalities or myopia of more than –6 diopter and did not have any systemic diseases. In six controls, imaging was performed in only one eye.

Image Acquisition

SD-OCT imaging (Spectralis HRA-OCT; Heidelberg Engineering) consisted of two OCT volumes covering the central macular area. These volumes each covered an area of 20 × 5 degrees (approximately 6 × 1.5 mm) with a distance of ~250 µm between seven B-scans. The OCT image size was 1024 × 7 × 496 voxels, and transverse and axial resolution was approximately 6 µm and 4 µm, respectively. The automatic real-time tracking was set to 25 frames per B-scan. The images were exported to DICOM format for analysis.

Image Segmentation

Automated segmentation of 11 different retinal surfaces was performed using the Iowa Reference Algorithm (Retinal Image Analysis Lab, Iowa Institute for Biomedical Imaging, Iowa City, IA, USA).[13–15] This resulted in 10 different retinal layer volumes. The following layer volumes were obtained: retinal nerve fiber layer (RNFL), ganglion cell layer (GCL), inner plexiform layer (IPL), inner nuclear layer (INL), outer plexiform layer, outer nuclear layer (ONL), inner photoreceptor segment (IS), outer photoreceptor segment (OS), photoreceptor outer segment, and the RPE combined with BM (see Supplementary Fig. S1). All B-scans were visually inspected for both integrity of the outer retinal layer and BM, as well as for correct segmentation of all retinal layers. If a part of the B-scan did not match these criteria, corresponding A-scans were excluded from further analysis. This was done by using the "Undefined Regions" tool of the Iowa Reference Algorithm (example in Supplementary Fig. S1). To prevent observer bias, incorrect segmentation was left unadjusted and excluded. The remainder of the total of 1024 A-scans per B-scan was used for further analysis. Coordinates of the surfaces and data on the included A-scans were saved as .xml files.

Image Processing

The OCT reflectivity and segmentation data were imported in MATLAB (version 9.1.0; MathWorks, Inc., Natick, MA, USA) using in-house built software. The exported images had an 8-bit precision, and the reflectivity values were transformed by the manufacturer to enhance visual contrast in areas with low reflectivity. This process was inversed to restore the original reflectivity values; the calibration curve is shown in Supplementary Figure S2. The retinal layer surface segmentations provide an estimate for the layer thickness in each A-scan. Linear interpolation was used to stretch the A-scan profiles, for each layer, to the same standardized length of twice the maximum layer thickness within the B-scan (see Supplementary Fig. S1B). For each included A-scan, we computed z-axis reflectivity profiles as a vector of 650 x-values. To calculate the median intensity profile for each layer, we first extracted the layer-specific reflectivity profiles from the stretched A-scans. Then, we calculated the median reflectivity profile by taking the median of all pixels at the same depth weighed to the original thickness of that A-scan. This was done in order to correct for local differences in layer thicknesses that might introduce measurement errors, such as the local thinning of the GCL in the foveal area. The median B-scan specific reflectivity was stored per row, resulting in 650 values per B-scan.

Image Analysis

We visualized the plotted reflectivity profiles using in-house built software. For this, the profiles were first averaged per OCT volume and then per patient. The reflectivity was normalized to the mean reflectivity of the GCL-IPL layer, unless otherwise stated. This layer is relatively far from the diseased outer retina and has a reasonable thickness. To enhance the contrast in areas with low reflectivity, the plots were rescaled to the fourth root of the normalized values.

We adhered to the nomenclature for outer retinal bands as proposed by Spaide and Curcio.[16] Therefore, we averaged the reflectivity of the IS and OS layers, which together form the ellipsoid zone (EZ) on the reflectivity profile. We used the layer-specific median and peak intensities for further analysis.

Subgroup Analysis

We excluded the A-scans with visible segmentation errors, but it is plausible that small errors remained. We used a subset of four patients with PXE and four controls to test the effect of small remaining errors in the segmentation algorithm. Of each person, we manually adjusted the segmentation in all seven B-scans in both the horizontal and vertical OCT scans and compared the reflectivity values and layer thickness to the original, unadjusted segmentation.

We tested the reproducibility of the reflectivity measurements in a subset of eight patients with PXE (30 OCT volumes) and four controls (16 OCT volumes). Repeated OCT scans were performed within a maximum of 6 months. We do not assume a significant progression of BM calcification within this time span. Eye-tracking technology was used to ensure that the exact same location was used for the follow-up scan. We extracted acquisition parameters such as scan focus, sensitivity, and image quality from the Heidelberg Eye Explorer to investigate their influence on agreement between repeated measures, as well as a visual inspection of the OCT scans (on motion artifacts or possible other disturbing phenomena).

Furthermore, we hypothesized that retinal vessels with shadowing artefacts might bias the measured RPE-BM reflectivity. These artifacts are caused by the retinal blood vessels in the GCL-IPL layers attenuating the signal. In A-scans with retinal blood vessels, this leads to a higher reflectivity in the GCL-IPL layer and a lower reflectivity in the RPE-BM layer. This effect is enlarged when the reflectivity is normalized. To

investigate the size of this possible effect, we used the before mentioned subset of eight patients with PXE and four controls in whom we repeated the image segmentation using the IOWA Reference Algorithm. Using the "Undefined Regions" tool, we excluded all A-scans with visible retinal vessels with shadowing artifacts, besides the before mentioned exclusion criteria.

Data Analysis

All values are presented as numbers with percentage (%), mean with standard deviation (± SD), or median with interquartile range (IQR). Distribution of values was tested with the Shapiro-Wilk test. Differences between groups were tested with Student's *t*-test, chi-square test, Mann-Whitney *U* test, or Kruskal-Wallis test when appropriate. Differences in the subgroup analyses were tested with paired *t*-test or Wilcoxon signed-rank test, when appropriate. To control for multiple testing, the *P* values of layer-specific analyses were adjusted according to Benjamini and Hochberg.[17]

Receiver operating characteristic (ROC) analysis was used to test discriminative performance of the RPE-BM reflectivity values, from which the area under the ROC curve (AUC) was calculated. The discriminative performances of the ROC curves were compared with the method as proposed by DeLong et al.[18] Spearman correlation analysis was used for correlation analysis. To investigate the correlation of reflectivity values between scans, we compared the left and right eyes for within-patient correlation and the horizontal and vertical OCT scan within the same eye for within-eye correlation. We visualized the agreement of the reflectivity between the repeated measurements in a plot proposed by Bland and Altman[19] and calculated the 95% limits of agreement.

Statistical analysis of the data was performed with R (version 3.4.1, The R Foundation, Vienna, Austria). The packages "pROC" (version 1.13.0) and "BlandAltmanLeh" (version 0.3.1) were used for ROC analysis and agreement analysis, respectively.[20]

Results

Of all 52 patients with PXE under 40 years (104 eyes), 11 eyes had retinal pathology, and an additional 18 eyes had a best-corrected visual acuity lower than 0.9 and were thus excluded from analysis. This resulted in OCT data of 75 eyes of 45 patients with PXE with a mean age of 27 years (range, 11–39 years) and 44 eyes of 25 normal controls with a mean age of 27 years (range, 14–39 years) (Table). The mean age was similar between the groups. Most patients with PXE were female (87%), compared with 56% females among controls ($P = 0.01$). The thickness of the reference layer was similar between patients with PXE and controls: the mean GCL-IPL thickness was 78 ± 4 µm in patients with PXE, compared with 77 ± 5 µm in controls ($P = 0.14$). In patients with PXE, the retina was 7 µm thinner than in controls, with statistically significant differences in the RNFL, INL, Ellipsoid zone (EZ), and RPE-BM layers. Layer specific thicknesses are presented in Supplementary Table S1.

Reflectivity Characteristics

The mean reflectivity profiles show differences in reflective bands of the retinal layers between PXE and controls (Fig. 1). The RPE-BM peak appears to be higher in patients with PXE. When quantified, the RPE-BM peak reflectivity was twice as high in patients with PXE (67.5; IQR, 42.1–84.2) as in controls (32.7; IQR, 25.7–38.9; adjusted $P = 2.43 \times 10^{-5}$). Consequently, the median reflectivity of the RPE-BM layer was higher in patients with PXE than in controls: 41.1 (IQR, 26.3–51.9) compared with 22.5 (IQR, 19.3–29.5; adjusted $P = 2.09 \times 10^{-3}$).The RPE-BM peak reflectivity performed best in distinguishing patients with PXE and controls with an AUC of 0.85 (95% CI, 0.76–0.95), compared with the RPE-BM median reflectivity with an AUC of 0.77 (95% CI, 0.66–0.88) ($P = 8.16 \times 10^{-5}$). The ROC curves are visualized in Figure 2. Furthermore, the median reflectivity of the photoreceptors of patients with PXE is lower than that of controls with nominal statistical significance but not when adjusted for multiple testing (Table).

Effect of Age

The RPE-BM peak reflectivity increased with age in patients with PXE but not in controls (Fig. 3). The RPE-BM peak reflectivity was 44.2 (IQR, 40.5–74.6) in patients with PXE under 20 years (n = 7), compared with 66.0 (IQR, 45.0–83.8) in patients aged 20 to 30 years (n = 22) and 70.8 (IQR, 49.0–88.0) in patients with PXE aged 30 to 40 years (n = 16). However, these differences were not statistically significant ($P = 0.48$). Median layer reflectivity also did not show statistically significant differences with increasing age. Detailed information can be found in Supplementary Table S2.

Within-Eye and Within-Patient Correlation

In patients with PXE, the RPE-BM peak reflectivity had a strong correlation between horizontal and vertical B-scans within the same eye ($\rho = 0.80$; adjusted

Table. Patient Characteristics and Layer Reflectivity

Characteristic	PXE (n = 45)	Control (n = 25)	Nominal *P*	Adjusted *P*[a]
Patient data				
Age, mean ± SD (years)	27 ± 7	27 ± 6	0.96	
Gender (male), *n* (%)	6 (13)	11 (44)	0.01	
Proportion of A-scans (%)	93 [92, 96]	95 [94, 96]	0.02	
Scan quality (dB), mean ± SD	35.2 ± 3.2	34.8 ± 2.6	0.64	
Median layer reflectivity				
Retinal nerve fiber layer	2.2 [2.0, 2.7]	2.3 [2.0, 2.6]	0.93	0.96
Ganglion cell layer	0.71 [0.67, 0.75]	0.69 [0.67, 0.73]	0.18	0.34
Inner plexiform layer	0.78 [0.73, 0.83]	0.79 [0.76, 0.82]	0.16	0.31
Inner nuclear layer	0.37 [0.32, 0.39]	0.36 [0.35, 0.40]	0.54	0.67
Outer plexiform layer	0.66 [0.56, 0.75]	0.69 [0.65, 0.78]	0.22	0.38
Outer nuclear layer	0.23 [0.19, 0.27]	0.24 [0.22, 0.28]	0.06	0.17
Ellipsoid zone	14.0 [8.3, 20.0]	17.2 [14.0, 27.0]	0.02	0.10
Outer photoreceptor segments	14.5 [9.1, 23.3]	21.7 [16.1, 29.7]	0.02	0.10
RPE and Bruch's membrane	41.1 [26.3, 51.9]	22.5 [19.3, 29.5]	1.90×10^{-4}	2.09×10^{-3}
Peak layer reflectivity				
Retinal nerve fiber layer	5.2 [4.3, 6.1]	4.7 [4.3, 6.5]	0.75	0.83
Ganglion cell layer	3.2 [2.9, 3.5]	3.1 [2.9, 3.4]	0.54	0.67
Inner plexiform layer	0.99 [0.92, 1.06]	0.99 [0.97, 1.05]	0.52	0.67
Inner nuclear layer	0.85 [0.76, 0.90]	0.82 [0.79, 0.92]	0.55	0.67
Outer plexiform layer	0.94 [0.78, 1.09]	0.97 [0.89, 1.08]	0.31	0.48
Outer nuclear layer	0.71 [0.61, 0.84]	0.77 [0.69, 0.96]	0.07	0.17
Ellipsoid zone	35.6 [24.4, 57.5]	40.6 [34.7, 59.4]	0.12	0.25
Outer photoreceptor segments	27.4 [17.5, 43.1]	38.2 [27.4, 56.3]	0.03	0.11
RPE and Bruch's membrane	67.5 [42.1, 84.2]	32.7 [25.7, 38.9]	1.10×10^{-6}	2.43×10^{-5}

All reflectivity values are normalized to the GCL-IPL layer. Values are presented as median [IQR] unless otherwise indicated.
[a]*P* values were adjusted according to the method as proposed by Benjamini and Hochberg.

$P < 2.2 \times 10^{-16}$; Fig. 4). For controls, this within-eye correlation was moderate ($\rho = 0.56$; adjusted $P = 1.03 \times 10^{-3}$). The within-patient correlation of the RPE-BM peak reflectivity between both eyes was moderate for patients with PXE and strong for controls ($\rho = 0.42$, adjusted $P = 0.03$ and $\rho = 0.71$, adjusted $P = 0.01$, respectively; Fig. 4).

The within-eye correlation for the median RPE-BM reflectivity was strong for patients with PXE (Spearman's $\rho = 0.77$; adjusted $P < 2.2 \times 10^{-16}$) and for controls ($\rho = 0.65$; adjusted $P = 1.06 \times 10^{-5}$). The within-patient correlation for the median RPE-BM reflectivity was moderate for patients with PXE ($\rho = 0.43$; adjusted $P = 0.03$) and strong for controls ($\rho = 0.68$; adjusted $P = 0.01$). Further details on within-eye and within-patient correlations of median layer reflectivity can be found in Supplementary Table S3.

Manual Correction of Segmentation

Manually adjusting all small segmentation errors in a subset of four patients with PXE (four eyes) and four controls (four eyes) did not result in statistically significant changes in the retinal layer thickness or in the GCL-IPL reflectivity (serving as the reference layer for normalization) or RPE-BM peak reflectivity (Supplementary Table S4). The correlation between RPE-BM peak reflectivity with and without adjusted segmentation for all OCT scans is visualized in Supplementary Figure S3. In this subset, the absolute difference of the RPE-BM peak reflectivity between PXE and controls becomes slightly larger: the absolute difference is 54 (95% CI, 22–80) for the unadjusted OCT scans, while this is 61 (95% CI, 27–84) for the adjusted OCT scans.

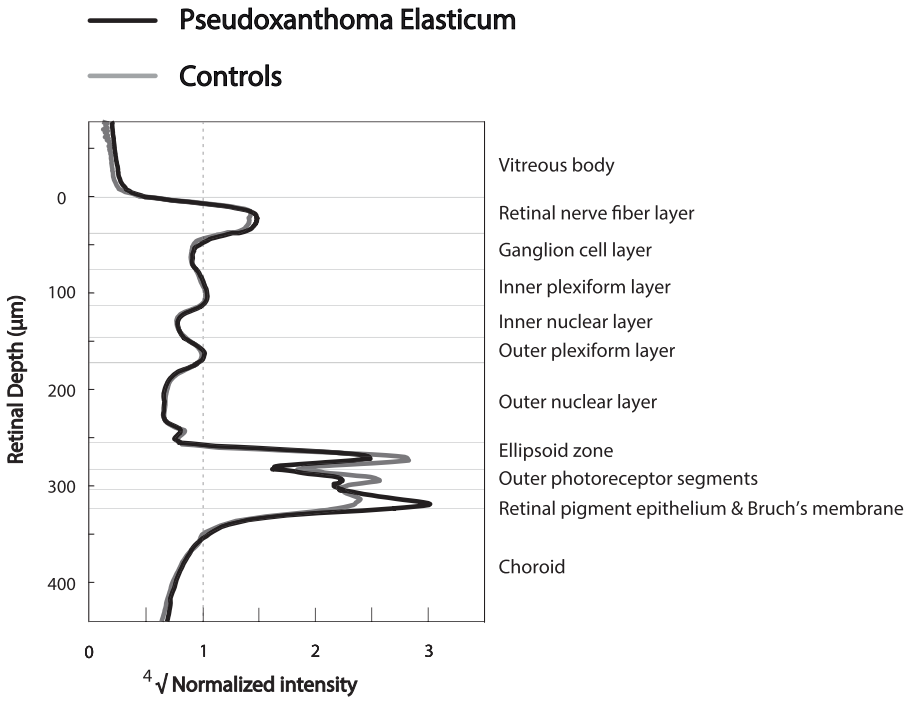

Figure 1. Reflectivity profiles of patients with PXE and controls. Averaged reflectivity profiles of patients with pseudoxanthoma elasticum (PXE) ($n = 45$) and controls ($n = 25$). The normalized reflectivity is plotted against the retinal depth. On the right side, the corresponding retinal layers are noted. The GCL-IPL layer was used as the reference layer for normalization. The fourth root of the normalized reflectivity was used for better visualization.

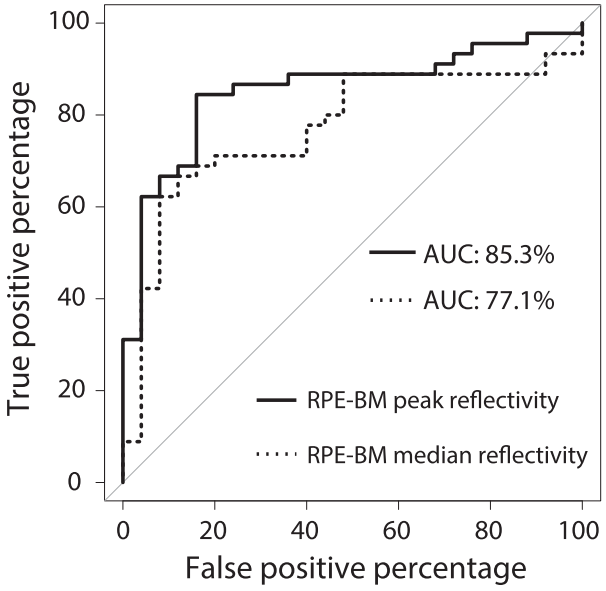

Figure 2. Receiver operating characteristic curve. ROC curve of the RPE-BM peak reflectivity and RPE-BM median reflectivity (normalized to the GCL-IPL layer). Reflectivity values were averaged per person.

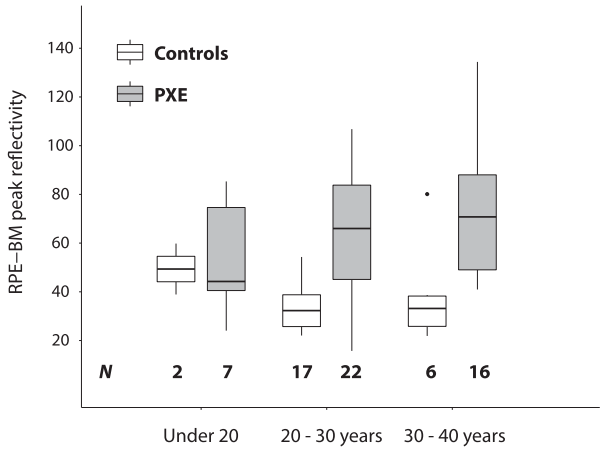

Figure 3. The effect of age. RPE-BM peak reflectivity of patients with PXE and controls, plotted by their age category. The RPE-BM reflectivity is normalized to the GCL-IPL layer. The *horizontal bars* represent the median value, and the *boxes* represent the interquartile range. Per person, the reflectivity values were averaged. The number of patients per category is listed at the bottom of the figure.

Reproducibility

We tested the reproducibility of the RPE-BM peak reflectivity in a subset of eight patients with PXE (15 eyes) and four controls (8 eyes). The agreement for the RPE-BM peak reflectivity, averaged per eye, is visualized in the Bland-Altman plot (Supplementary Fig. S4). The mean absolute difference between the first and second measurements was 13.7 for patients with

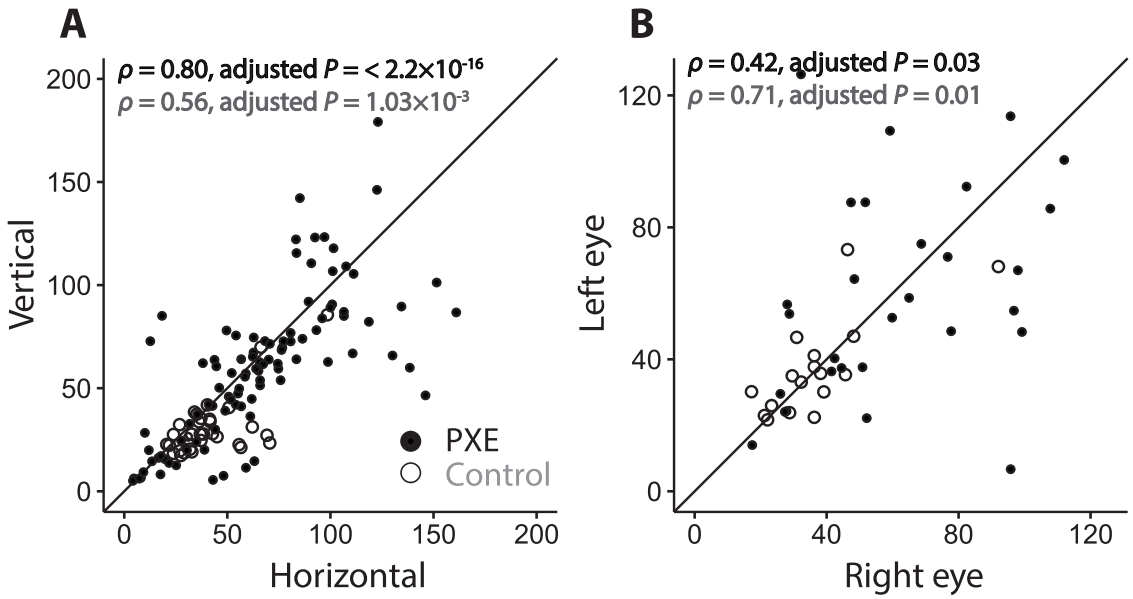

Figure 4. Within-eye and within-subject correlation. Within-eye (A) and within-subject (B) correlation of RPE-BM peak reflectivity of patients with PXE and controls. Within-eye correlation is measured with horizontally and vertically orientated OCT scans. For within-eye correlation, there were 101 comparisons for patients with PXE and 36 comparisons for controls. For within-subject correlation, there were 29 pairs of observation in patients with PXE and 19 pairs of observation in controls. The *diagonal line* represents the perfect correlation. In the *top-left* corner, the Spearman correlation coefficients (ρ) are shown for patients with PXE (*black*) and controls (*gray*).

PXE and –1.8 for controls. The 95% limits of agreement were –53.0 and 79.5 for patients with PXE and –34.2 and 30.5 for controls. In this subset, the acquisition parameters scan focus, sensitivity, and image quality were not associated with the GCL-IPL reflectivity, which was used for normalization, or with the reproducibility.

Shadowing Artifacts

Excluding all A-scans with retinal blood vessels and shadowing artefacts on the B-scan from analysis resulted in a statistically significant lower proportion of included A-scans: 83.3% ± 5.8% A-scans per B-scan while excluding retinal blood vessels versus 93.7% ± 5.7% in normal segmentation ($P < 2.2 \times 10^{-16}$). The RPE-BM peak reflectivity was slightly higher if retinal blood vessels were excluded: the median difference in patients with PXE was 1.20 (95% CI, 0.8–1.6; $P = 1.65 \times 10^{-6}$) and 0.8 (95% CI, 0.6–1.2; $P = 4.21 \times 10^{-7}$) in controls. The absolute difference in RPE-BM peak reflectivity in patients with PXE and controls remained the same: 48.0 (95% CI, 38.3–61.1) if A-scans with retinal blood vessels were excluded versus 47.5 (95% CI, 37.9–61.1) with normal segmentation.

Discussion

To our knowledge, this is the first study on the reflectivity characteristics of SD-OCT in patients with PXE. We found that the reflectivity profiles of relatively young patients with PXE are different from controls and that the RPE-BM peak reflectivity performs well in discriminating patients with PXE from controls.

Our findings confirm previous observations of OCT imaging in PXE, which describe increased reflectivity at the level of the RPE-BM complex.[3,6,21,22] This finding is also compatible with the histopathologic evidence of calcification in BM.[23] The increased reflective properties of the calcified BM cause the hyperreflectivity of the RPE-BM complex on SD-OCT, which appears to correlate with its bright reflex on near-infrared imaging.[7] Besides near-infrared imaging, late-phase indocyanine green angiography also visualizes the pattern of BM calcification.[24,25] However, quantification methods for these retinal imaging techniques are not available yet. The distance between the temporal border of the optic disc and the central border of peau d'orange has been used as a proxy for the extent of calcification.[26] The eccentricity of the border of the peau d'orange may provide relevant information

regarding the progression of the extent of BM calcification, but it is unclear whether this parameter also represents severity of retinal calcification.[26] A recent study showed reduced quantitative autofluorescence in PXE, which suggests reduced lipofuscin levels within the RPE.[27] These levels were associated with the extent of calcification, implicating that BM calcification in PXE affects the vitality of the outer retina.

In this study, we investigated the use of SD-OCT reflectivity values, normalized to the GCL-IPL reference layer, as a quantifiable biomarker for PXE. Quantification of reflectivity values is hardly used, in contrast to quantification of layer thickness, because interpretation of reflectivity values is less straightforward. Since the reflectivity values are influenced by multiple factors such as media opacities and signal-to-noise ratio and SD-OCT imaging is not calibrated, absolute reflectivity values are not considered a reliable metric.[8] Approaches to obtain reliable reflectivity data include normalization to image quality or signal strength, to a reference layer, or by using an attenuation coefficient.[11,28] The RNFL or RPE has been suggested as the best reference layer, since these layers show the highest reflectivity values.[29] On the other hand, the ONL, which shows the lowest reflectivity values in the retina, has been proposed because of the best correlation with image quality.[8] For the purpose of our study, both candidates are not ideal; the macular RNFL is rather thin, and normalizing the high RPE-BM reflectivity to the low ONL reflectivity could result in a biomarker that is extremely sensitive to measurement errors in the reference layer having a low signal-to-noise ratio.[8] Moreover, the ONL represents the nuclear bodies of the photoreceptor cells, which theoretically will suffer first from a diseased RPE-BM complex in PXE. The GCL-IPL layer is, besides the RNFL, furthest away from the outer retina, and the thickness and reflectivity values of the GCL-IPL layer allow for easy segmentation. Only in the foveal area does the GCL-IPL layer almost diminish, which likely causes noise in the reference layer reflectivity. Therefore, we selected the GCL-IPL layer as a reference layer corrected for the foveal thinning by weighing the reflectivity profiles to the layer thickness to normalize the reflectivity values.

We observed a large variability in normalized reflectivity values, both between patients and within patients. The high variability between patients might partly be explained by age and the severity of the disease. However, this does not explain the variability within patients and thus the low reproducibility. It is in line with a study that found that reflectivity values may vary up to 29% due to sensitivity fall-off (decreasing sensitivity with increasing retinal depth) and patient-induced motions, such as a heartbeat, that cause axial shift.[30] Also, a change in the angle of the infrared light beam affects the reflectivity and attributes to the variability of measured reflectivity.[31] Therefore, it is complicated to obtain a reproducible measure of OCT reflectivity, which is often prone to substantial intrapatient variation.[32] Unfortunately, our data set with repeated measures was rather small and lacked statistical power to investigate the reproducibility more in depth. Future research should therefore focus on gaining insight into and improving reproducibility. Progress in OCT technology, such as the introduction of the Spectralis OCT2, providing faster imaging with a higher signal-to-noise ratio, is expected to be beneficial for improving the reproducibility.[33] Also, another approach for normalizing the reflectivity may be worth investigating. The approach proposed by Vermeer et al.[34] could be valuable, since it does not rely on a reference layer but uses a pixel-specific attenuation coefficient to characterize the retinal tissue. Even though we cannot use the RPE-BM reflectivity as an individual biomarker yet, the RPE-BM reflectivity is a reliable parameter to compare groups with a random measurement error.

We could not demonstrate a statistically significant effect of age on the RPE-BM peak reflectivity. It is known that BM calcification in PXE increases with age and is hypothesized to spread centrifugally.[25] Gliem et al.[27] recently found that the extent of calcification increases with age but has a large between-patient variability. Interestingly, our data also suggest a possible trend of increasing RPE-BM peak reflectivity with increasing age. However, we should take into account that we only measured patients aged under 40 years, and thus the reflectivity throughout life is still unknown. Moreover, it is plausible that the large variability between patients and the relatively small sample size impede reaching statistical significance. Also, it is likely that the excluded patients with PXE with CNV or macular atrophy had more severe BM calcification than patients with PXE of the same age without these complications. It would therefore be interesting to study the hypothesis that the RPE-BM peak reflectivity in PXE increases with age by including older and more severe patients with PXE or by increasing the study population. However, even though our findings provide convincing evidence that we can detect BM calcification in PXE already at a young age and may suggest that the BM calcification progresses with age, the characteristics of the RPE-BM peak reflectivity need to be validated in an external cohort of patients with PXE. Also, there was a substantial and at this moment unexplained variability between patients,

which is known from other measures in patients with PXE.[27] Therefore, before the RPE-BM peak reflectivity is suitable as a longitudinal biomarker, the reproducibility needs to be improved.

Changes in BM also occur with normal aging, which means that BM calcification in PXE may represent a part of the normal aging process. Also, the RPE reflectivity increases with age, which is attributed to enlarged melanosomes in the RPE.[35] Since BM is very thin, it is hard to investigate the BM reflectivity separate from the RPE reflectivity. Both phenomena, however, cannot explain the observed difference in RPE-BM peak reflectivity between patients with PXE and controls.

Furthermore, changes in BM occur as part of the pathophysiology of AMD.[36,37] AMD may progress to a neovascular or atrophic stage due to changes in the anatomical complex consisting of the photoreceptors, RPE-BM, and the choriocapillaris.[36] Patients with AMD also have a different OCT reflectivity profile: the ellipsoid zone has a lower reflectivity than controls, which correlates with retinal function.[38] Possibly, the OCT reflectivity profile also shows differences in the RPE-BM complex due to BM calcification or other changes in the complex consisting of choriocapillaris, RPE-BM, and the photoreceptors.[39] Therefore, OCT reflectivity profiles may be an interesting biomarker to monitor early changes in patients with AMD or even as a screening tool for detection of early AMD.[40]

Interestingly, we also found an indication that patients with PXE have a lower photoreceptor reflectivity than controls, with nominal statistical significance (Table). The interpretation is yet uncertain. An altered optical Stiles Crawford effect may contribute to this difference between patients with PXE and controls. The optical Stiles-Crawford effect describes the phenomenon that OCT reflectivity depends on the directionality of the retinal tissue.[41] The directionality of the photoreceptors might be altered by retinal pathophysiology, which then leads to an altered absorption and reflection of light.[42] Possibly, BM calcification affects the directionality of the photoreceptors and thereby its reflectivity. However, it is also plausible that BM calcification affects the vitality of the photoreceptors by impeding the diffusion of nutrients and oxygen from the choriocapillaris. This may then cause photoreceptor dysfunction and degeneration. Despite the lack of large-scale studies providing convincing evidence, the existing literature indicates that patients with PXE have impaired retinal function. Three studies in 35, 15, and 4 patients with PXE found reduced retinal function or dark adaptation, which supports this hypothesis.[43–45] However, one study did not find retinal dysfunction in seven patients with PXE.[46] Future research should compare retinal function with OCT reflectivity to further investigate the mechanism of lower photoreceptor reflectivity in patients with PXE.

Moreover, we found differences in thickness of the total retina and in several retinal layers. Two previous studies reported on a lower retinal thickness in eyes with PXE, but these studies included later stages of PXE with CNV and/or atrophy, making it difficult to compare our findings.[47,48] Since there are no data on retinal layer thickness in PXE, it is difficult to interpret these findings. Perhaps BM calcification already affects the thickness of some retinal layers at an early disease stage. However, it is also very plausible that the segmentation algorithm attributed to the differences in layer thickness. The IOWA segmentation algorithms rely on signal strength and the higher RPE-BM reflectivity in patients with PXE may slightly affect the algorithm.[49] Last, the method of thickness measurements differs from commonly used methods (e.g., measuring along the length of the standardized Early Treatment of Diabetic Retinopathy (ETDRS) grid). Both the uncertainty regarding why the layers differ in thickness, as well as the method of measurement, should be taken into account when interpreting or comparing the retinal layer thicknesses.

Some limitations need to be addressed. The IOWA reference algorithms that we used to segment the retinal layers are based on a three-dimensional approach, which models the surfaces of retinal layers, whereas our OCT volumes consist of seven B-scans. This might result in small segmentation errors at the fovea. However, in this study, all B-scans were visually inspected, and in case there were clearly visible segmentation errors, the A-scans in that area were excluded. Also, manual adjustment of small segmentation errors did not affect the results; the small, nonsignificant changes are seen in both patients with PXE and controls, and they follow the same direction. They will thus not weaken the differences seen between PXE and controls. Therefore, we do not assume that this has affected the validity of our findings. Then, the RPE-BM peak reflectivity might have been slightly affected in patients with PXE due to the presence of angioid streaks that were not detectable on OCT. In most cases, however, angioid streaks are visible on OCT as breaks in BM,[7] and we excluded those A-scans with our approach. This resulted in a lower proportion of included A-scans per B-scan in patients with PXE compared with controls. Hypothetically, undetected angioid streaks could lower RPE-BM peak reflectivity, but we assume that the proportion of A-scans with undetected streaks is so small that a large effect on reflectivity values is unlikely. At last, we found that the shadowing artifacts of retinal blood vessels affected

the RPE-BM reflectivity, but this effect was relatively small and did not influence the large difference between reflectivity in patients with PXE and controls. However, it does indicate that the RPE-BM reflectivity might be slightly affected by above lying structures. To prevent this, an approach based on attenuation coefficients could be an option in future research.

In conclusion, we showed that patients with PXE have increased normalized RPE-BM reflectivity, presumably as a result of BM calcification. The normalized RPE-BM peak reflectivity has potential to be the first biomarker for the severity of BM calcification in patients with PXE. This finding is relevant to gain insight not only into PXE pathology but into normal aging and AMD as well. Further research is warranted to confirm our findings and to further improve the reproducibility of the RPE-BM peak reflectivity.

Acknowledgments

The authors thank Kyungmu Lee for his support with the automated segmentation, Ruud Groenleer for his support with the export of data, Michel Teussink for supporting us with our technical approach, and Johannes H. de Boer for proofreading the manuscript.

Supported by unrestricted grants from the F.P. Fischer Stichting, Rotterdamse Stichting Blindenbelangen, Stichting Vrienden UMC Utrecht, and Stichting PXE-Fonds, which had no role in the design or conduct of this research.

Disclosure: **S. Risseeuw,** None; **E. Bennink,** None; **M.G. Poirot,** None; **P.A. de Jong,** None; **W. Spiering,** None; **S.M. Imhof,** None; **R. van Leeuwen,** None; **J. Ossewaarde-van Norel,** None

References

1. Bergen AA, Plomp AS, Schuurman EJ, et al. Mutations in ABCC6 cause pseudoxanthoma elasticum. *Nat Genet*. 2000;25:228–231.
2. Kranenburg G, Baas AF, de Jong PA, Asselbergs FW, Visseren FLJ, Spiering W. The prevalence of pseudoxanthoma elasticum: revised estimations based on genotyping in a high vascular risk cohort. *Eur J Med Genet*. 2019;62:90–92.
3. Gliem M, De Zaeytijd, J, Finger RP, Holz FG, Leroy BP, Charbel Issa P. An update on the ocular phenotype in patients with pseudoxanthoma elasticum. *Front Genet*. 2013;4:14.
4. Risseeuw S, Ossewaarde-van Norel J, Klaver CCW, Colijn JM, Imhof SM, van Leeuwen R. Visual acuity in pseudoxanthoma elasticum. *Retina*. 2019;39:1580–1587.
5. Kranenburg G, de Jong PA, Bartstra JW, et al. Etidronate for prevention of ectopic mineralization in patients with pseudoxanthoma elasticum. *J Am Coll Cardiol*. 2018;71:1117–1126.
6. Spaide RF. Peau d'orange and angioid streaks: manifestations of Bruch membrane pathology. *Retina*. 2015;35:392–397.
7. Charbel Issa P, Finger RP, Holz FG, Scholl HPN. Multimodal imaging including spectral domain OCT and confocal near infrared reflectance for characterization of outer retinal pathology in pseudoxanthoma elasticum. *Invest Ophthalmol Vis Sci*. 2009;50:5913–5918.
8. Chen X, Hou P, Jin C, et al. Quantitative analysis of retinal layer optical intensities on three-dimensional optical coherence tomography. *Invest Ophthalmol Vis Sci*. 2013;54:6846–6851.
9. Ramrattan RS, Van der Schaft TL, Mooy CM, De Bruijn WC, Mulder PGH, De Jong, PTVM. Morphometric analysis of Bruch's membrane, the choriocapillaris, and the choroid in aging. *Investig Ophthalmol Vis Sci*. 1994;35:2857–2864.
10. Chen C-L, Ishikawa H, Wollstein G, et al. Individual A-scan signal normalization between two spectral domain optical coherence tomography devices. *Investig Opthalmology Vis Sci*. 2013;54:3463.
11. Vermeer KA, van der Schoot J, Lemij HG, de Boer JF. RPE-normalized RNFL attenuation coefficient maps derived from volumetric OCT imaging for glaucoma assessment. *Investig Opthalmol Vis Sci*. 2012;53:6102.
12. Plomp AS, Toonstra J, Bergen AAB, van Dijk MR, de Jong, PTVM. Proposal for updating the pseudoxanthoma elasticum classification system and a review of the clinical findings. *Am J Med Genet A*. 2010;152:1049–1058.
13. Garvin MK, Abràmoff MD, Wu X, Russell SR, Burns TL, Sonka M. Automated 3-D intraretinal layer segmentation of macular spectral-domain optical coherence tomography images. *IEEE Trans Med Imaging*. 2009;28:1436–1447.
14. Antony B, Abràmoff MD, Tang L, et al. Automated 3-D method for the correction of axial artifacts in spectral-domain optical coherence tomography images. *Biomed Opt Express*. 2011;2:2403–2416.
15. Li K, Wu X, Chen DZ, Sonka M. Optimal surface segmentation in volumetric images—a graph-

theoretic approach. *IEEE Trans Pattern Anal Mach Intell*. 2006;28:119–134.
16. Spaide RF, Curcio CA. Anatomical correlates to the bands seen in the outer retina by optical coherence tomography: literature review and model. *Retina*. 2011;31:1609–1619.
17. Benjamini Y, Hochberg Y. Controlling the false discovery rate: a practical and powerful approach to multiple testing. *J R Stat Soc Ser B*. 1995;57:289–300.
18. DeLong ER, DeLong DM, Clarke-Pearson DL. Comparing the areas under two or more correlated receiver operating characteristic curves: a nonparametric approach. *Biometrics*. 1988;44:837–845.
19. Bland JM, Altman DG. Statistical methods for assessing agreement between two methods of clinical measurement. *Lancet*. 1986;1:307–310.
20. Robin X, Turck N, Hainard A, et al. pROC: an open-source package for R and S+ to analyze and compare ROC curves. *BMC Bioinformatics*. 2011;12:77.
21. Ari Yaylali S, Akcakaya AA, Erbil HH, Salar S, Karakurt Y. Optical coherence tomography findings in pseudoxanthoma elasticum. *Eur J Ophthalmol*. 2010;20:397–401.
22. Charbel Issa P, Finger RP, Holz FG, Scholl HPN. Multimodal imaging including spectral domain OCT and confocal near infrared reflectance for characterization of outer retinal pathology in pseudoxanthoma elasticum. *Investig Opthalmol Vis Sci*. 2009;50:5913.
23. Jensen OA. Bruch's membrane in pseudoxanthoma elasticum. Histochemical, ultrastructural, and x-ray microanalytical study of the membrane and angioid streak areas. *Albrecht Von Graefes Arch Klin Exp Ophthalmol*. 1977;203:311–320.
24. De Zaeytijd J, Vanakker OM, Coucke PJ, De Paepe A, De Laey J-J, Leroy BP. Added value of infrared, red-free and autofluorescence fundus imaging in pseudoxanthoma elasticum. *Br J Ophthalmol*. 2010;94:479–486.
25. Charbel Issa P, Finger RP, Gotting C, Hendig D, Holz FG, Scholl HPN. Centrifugal fundus abnormalities in pseudoxanthoma elasticum. *Ophthalmology*. 2010;117:1406–1414.
26. Gliem M, Hendig D, Finger RP, Holz FG, Charbel Issa P. Reticular pseudodrusen associated with a diseased Bruch membrane in pseudoxanthoma elasticum. *JAMA Ophthalmol*. 2015;133:581–588.
27. Gliem M, Müller PL, Birtel J, et al. Quantitative fundus autofluorescence in pseudoxanthoma elasticum. *Investig Ophthalmol Vis Sci*. 2017;58:6159–6165.
28. Sun M, Zhang Z, Ma C, Chen S, Chen X. Quantitative analysis of retinal layers on three-dimensional spectral-domain optical coherence tomography for pituitary adenoma. *PLoS One*. 2017;12:e0179532.
29. Neudorfer M, Weinberg A, Loewenstein A, Barak A. Differential optical density of subretinal spaces. *Invest Ophthalmol Vis Sci*. 2012;53:3104–3110.
30. Teussink MM, Cense B, van Grinsven MJJP, Klevering BJ, Hoyng CB, Theelen T. Impact of motion-associated noise on intrinsic optical signal imaging in humans with optical coherence tomography. *Biomed Opt Express*. 2015;6:1632–1647.
31. Huang X-R, Knighton RW, Feuer WJ, Qiao J. Retinal nerve fiber layer reflectometry must consider directional reflectance. *Biomed Opt Express*. 2016;7:22.
32. Mehta N, Lavinsky F, Gattoussi S, et al. Increased inner retinal layer reflectivity in eyes with acute CRVO correlates with worse visual outcomes at 12 months. *Investig Opthalmol Vis Sci*. 2018;59:3503.
33. Bosche F, Andresen J, Li D, Holz F, Brinkmann C. Spectralis OCT1 versus OCT2: time efficiency and image quality of retinal nerve fiber layer thickness and Bruch's membrane opening analysis for glaucoma patients. *J Curr Glaucoma Pract*. 2019;13:16–20.
34. Vermeer KA, Mo J, Weda JJA, Lemij HG, de Boer JF. Depth-resolved model-based reconstruction of attenuation coefficients in optical coherence tomography. *Biomed Opt Express*. 2013;5:322–337.
35. Chen B, Gao E, Chen H, et al. Profile and determinants of retinal optical intensity in normal eyes with spectral domain optical coherence tomography. *PLoS One*. 2016;11:e0148183.
36. Bhutto I, Lutty G. Understanding age-related macular degeneration (AMD): relationships between the photoreceptor/retinal pigment epithelium/Bruch's membrane/choriocapillaris complex. *Mol Aspects Med*. 2012;33:295–317.
37. Booij JC, Baas DC, Beisekeeva J, Gorgels TGMF, Bergen AAB. The dynamic nature of Bruch's membrane. *Prog Retin Eye Res*. 2010;29:1–18.
38. Wu Z, Ayton LN, Guymer RH, Luu CD. Relationship between the second reflective band on optical coherence tomography and multifocal electroretinography in age-related macular degeneration. *Investig Opthalmol Vis Sci*. 2013;54:2800.
39. Reumueller A, Schmidt-Erfurth U, Salas M, et al. Three-dimensional adaptive optics—assisted visualization of photoreceptors in healthy and pathologically aged eyes. *Investig Opthalmol Vis Sci*. 2019;60:1144.

40. Garcia Garrido M, Beck SC, Mühlfriedel R, Julien S, Schraermeyer U, Seeliger MW. Towards a quantitative OCT image analysis. *PLoS One*. 2014;9:e100080.
41. Snyder AW, Pask C. The Stiles-Crawford effect-explanation and consequences. *Vision Res*. 1973;13:1115–1137.
42. DeLint PJ, Berendschot TTJM, Van Norren D. A comparison of the optical Stiles-Crawford effect and retinal densitometry in a clinical setting. *Investig Ophthalmol Vis Sci*. 1998;39:1519–1523.
43. Audo I, Vanakker OM, Smith A, et al. Pseudoxanthoma elasticum with generalized retinal dysfunction, a common finding? *Investig Opthalmol Vis Sci*. 2007;48:4250.
44. François J, De Rouck A. Electrophysiological Studies in Groenblad-strandberg Syndrome. In: Schmöger E, Kelsey JH (eds) *Visual Electrodiagnosis in Systemic Diseases. Documenta Ophthalmologica Proceeding Series*, vol 23. Springer, Dordrecht; 1980.
45. Hess K, Gliem M, Birtel J, et al. Impaired dark adaptation associated with a diseased Bruch membrane in pseudoxanthoma elasticum [published online December 10, 2019]. *Retina*.
46. Holz FG, Jubb C, Fitzke FW, Bird AC, Pope FM. Dark adaptation and scotopic perimetry over "peau d'orange" in pseudoxanthoma elasticum. *Br J Ophthalmol*. 1994;78:79–80.
47. Dolz-Marco R, Andreu-Fenoll M, Hernández-Martínez P, Pinazo-Durán MD, Gallego-Pinazo R. Automated macular choroidal thickness measurement by swept-source optical coherence tomography in pseudoxanthoma elasticum. *Int J Retin Vitr*. 2016;2:15.
48. Ellabban AA, Tsujikawa A, Matsumoto A, et al. Macular choroidal thickness and volume in eyes with angioid streaks measured by swept source optical coherence tomography. *Am J Ophthalmol*. 2012;153:1133–1143.
49. Darma S, Kok PHB, van den Berg, TJTP, et al. Optical density filters modeling media opacities cause decreased SD-OCT retinal layer thickness measurements with inter- and intra-individual variation. *Acta Ophthalmol*. 2015;93:355–361.